Affinity driven ion exchange EG-OFET sensor for high selectivity and low limit of detection of Cesium in seawater

Tin Phan Nguy, Volkan Kilinc, Ryoma Hayakawa, Catherine Henry-De-Villeneuve, Jean-Manuel Raimundo, Yutaka Wakayama, Anne Charrier

▶ **To cite this version:**

Tin Phan Nguy, Volkan Kilinc, Ryoma Hayakawa, Catherine Henry-De-Villeneuve, Jean-Manuel Raimundo, et al.. Affinity driven ion exchange EG-OFET sensor for high selectivity and low limit of detection of Cesium in seawater. Sensors and Actuators B: Chemical, 2022, 351, pp.130956. 10.1016/j.snb.2021.130956 . hal-03395388v2

HAL Id: hal-03395388
https://hal.science/hal-03395388v2

Submitted on 9 Dec 2021

HAL is a multi-disciplinary open access archive for the deposit and dissemination of scientific research documents, whether they are published or not. The documents may come from teaching and research institutions in France or abroad, or from public or private research centers.

L'archive ouverte pluridisciplinaire **HAL**, est destinée au dépôt et à la diffusion de documents scientifiques de niveau recherche, publiés ou non, émanant des établissements d'enseignement et de recherche français ou étrangers, des laboratoires publics ou privés.

Distributed under a Creative Commons Attribution - NonCommercial - NoDerivatives 4.0 International License

SENSORS & ACTUATORS B: CHEMICALS

https://doi.org/10.1016/j.snb.2021.130956

Sensors & Actuators: B. Chemical 351 (2022) 130956

Affinity driven ion exchange EG-OFET sensor for high selectivity and low limit of detection of Cesium in seawater

Tin Phan Nguy[1,2*], Volkan Kilinc[1,3*], Ryoma Hayakawa[1], Catherine Henry-de-Villeneuve[4], Jean-Manuel Raimundo[3#,$], Yutaka Wakayama[1,2#,$], Anne Charrier[3#,$]

[1] *International Center for Materials Nanoarchitectonics (WPI-MANA), National Institute for Materials Science (NIMS), 1-1 Namiki, Tsukuba 305-0044, Japan*

[2] *Department of Chemistry and Biochemistry, Faculty of Engineering, Kyushu University, 1-1 Namiki, Tsukuba 305-0044, Japan*

[3] *Aix Marseille Univ, CNRS, CINaM, Marseille, France*

[4] *Laboratoire de Physique de la Matière Condensée, CNRS, Ecole Polytechnique, Institut Polytechnique de Paris, 91120 Palaiseau, France*

Keywords: OFET, Cesium detection, Calix[4]arene, Selectivity in competitive media, Affinity, P3HT, Lipid monolayer, ultra-thin organic layers

[*] Authors contributed equally to the work
[#] Authors contributed equally to the work
[$] Corresponding author: raimundo@cinam.univ-mrs.fr
[$] Corresponding author: Wakayama.Yutaka@nims.go.jp
[$] Corresponding author: anne.charrier@univ.amu.fr

ABSTRACT

The detection and quantification of Cs^+ in aquatic media are an environmental safety and public health matter, so far limited by the lack of rapid, low cost, low limit of detection and selective analytical tools. Herein we demonstrate the efficient fabrication of a novel electrolyte-gated organic field-effect transistor sensor for the Cs^+ detection in seawater based on the combination of two ultra-thin layers namely poly(3-hexylthiophene) as semiconductor and a single lipids monolayer as dielectric. The latter is end-capped with a specific Cs^+ probe based on a calix[4]arene benzocrown ether to ensure the selectivity. Interestingly, we clearly evidence that by controlling affinity driven guest/host ion exchange, one can lift the general problem of selectivity encountered in all FET-based ion sensors, reaching a nearly perfect selectivity even in highly complex analyte solutions containing competitive ions, such as phosphate buffered saline solution or seawater. Such ultra-thin transistor structure exhibits, a limit of detection at the sub-femtomolar level which corresponds to a 5 folds' magnitude lower than Inductively Coupled Plasma Mass Spectroscopy, the most commonly used technic today. These results pave the way to a generalized monitoring of Cs^+ in complexed analytes.

1. Introduction

Regular and systematic monitoring of radioactivity levels in natural waters is of crucial importance and a matter of public health, and is still limited by the lack of rapid and low-cost on-site analytical tools. The largest sources of aquatic pollution originate from cesium isotopes from nuclear waste and industrial landfills. The two most prominent cesium radioisotopes, 134 and 137, are particularly problematic both due to their high half-life and solubility in water which facilitates their spread by air or sea [1]. Thus, ten years after the Fukushima accident in 2011, the quantities of cesium, which occurs naturally in seawater at concentration in the range 0.03-0.05 ng/l (~300 fM) [2], have doubled locally, but also in regions several thousand kilometers away impacting the global environment [3–6]. The health standards set by the governments vary country to country and are often dictated by the detection limits of the analytical tools. For instance, the European standard for drinking mineral water and dairy products is 300 Bq/kg [7,8],

which fits with the low limit of detection of the Inductively Coupled Plasma Mass Spectroscopy (ICP-MS) technique, providing to date the most sensitive and accurate results (limit of detection of 2 pM) [9]. In other countries such as Japan and Eastern European countries, where this standard is lowered to 10 Bq/kg and 50 Bq/kg for drinking water and dairy products respectively [10], analysis is hence conditioned to product pre-concentration.

Confronted to this need in large scale and low concentration Cs^+ monitoring in aquatic media and soils, much effort has been made to develop new, transportable, low-cost, immediate-response devices. Optical detection induced by cesium complexation appears to be one of the most favorite strategies [11,12]. A set of devices based on colorimetric detection using gold nanoparticles and Prussian blue [13], chrysoidine G as chemo indicator [14] or an optode based on ion-exchange membrane [15] allow naked eyes detection at the micromolar level. Fluorescence detection using squaraine fluorophore resulted in a significant lowering of the limit of detection down to 130 nM [16]. In another study, seawater was exposed to high energy micro discharge, from which Cs^+ could be determined at concentrations as low as 100 pM by recording the emission spectrum [17]. Besides, carbon electrodes modified with Clinoptilolite nanoparticles [18] or self -assembled thiacalix[4]arene on gold surfaces [19] were successfully developed for electrochemical Cs^+ detection. Although selective and low cost, these techniques present a limit of detection which is not sufficiently low to address the requirements for a real-time detection in aquatic media, natural waters or drinkable products. Only recently, a sensor based on water-gated thin film transistor (WGTFT), with a channel formed by a spray-pyrolyzed tin dioxide SnO_2 coated with a doped-PVC membrane with a cesium-selective zeolite "mordenite", was reported allowing the detection of cesium in drinking water at a concentration down to 33 fM [20]. Furthermore, electrolyte gated Field-effect transistors (EG-FET) sensors which have already demonstrated to provide very low limit of detection for ions [21–24] hence have emerged to be a promising and reliable technology. However, the detection of ions in complex analytes with high ionic strength such as in seawater is still challenging: selectivity is impeded by the presence of interfering ions; the presence of small cations such as potassium and sodium which are well known to act as electrical traps for FETs

[25–28] are very likely to lead to transistor performance degradation; finally, small Debye length is expected to reduce the sensitivity of the sensor by charge screening.

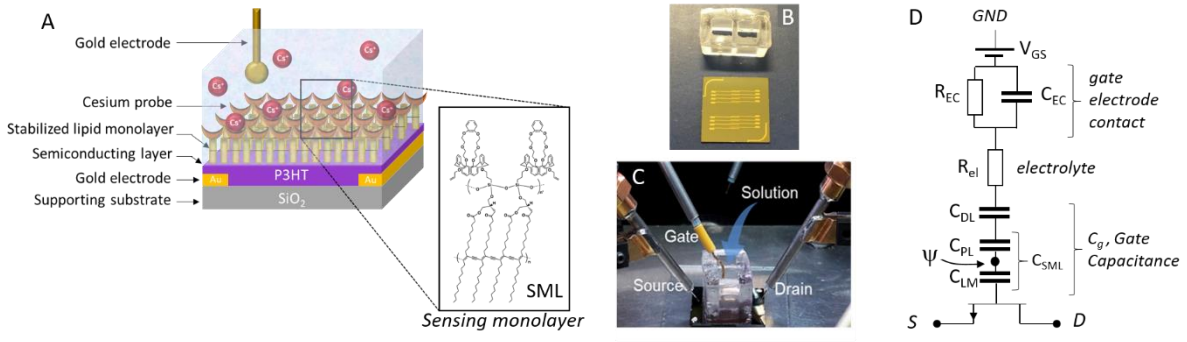

Figure 1: A) EG-OFET sensor design based on ultra-thin layers of P3HT and engineered lipid monolayer as semiconducting and dielectric materials respectively. The Cesium probe is a calix[4]arene benzocrown ether grafted to the lipid monolayer through a triethoxysilane groups. B) Picture of a chip containing 8 transistors mounted in parallel. C) Picture of the set-up for electrical measurements. D) Equivalent circuit of the system representing the sensing monolayer/electrolyte interface, the electrolyte and the gate electrode/electrolyte interface.

In this manuscript, we will demonstrate that by selecting the right transistor components, one can overcome most of these limitations. We describe the fabrication of a new type FET-based sensor, consisting of ultra-thin active layers, which can be easily integrated and miniaturized for on-site measurements, with immediate response and low power consumption (Fig. 1). This all-organic transistor consists of a 20 nm thin film of poly(3-hexylthiophene) semiconductor polymer (P3HT) and a 2.2 nm thick lipid monolayer as the gate dielectric. P3HT has a reasonable carrier mobility (10^{-4} - 10^{-1} cm^2V^{-1} s^{-1}) and has the great advantage to form perfectly flat films with low roughness, hence facilitating the formation of dense and compact lipid monolayers at its interface [29]. It was also shown that the formation of the lipid monolayer on top of P3HT is not affecting strongly (same order of magnitude) its carrier mobility [30]. The lipid layers have been engineered by a double cross-linking process which allows their stabilization and a high resistance to mechanical and electrical stresses [31–33]. The combination of P3HT film and lipid monolayer, has recently been used in the manufacture of electrolyte gated organic transistors (EG-OFETs) as pH sensors and has been shown to be effective in stabilizing the transistor response and increasing its lifetime

by preventing doping by ions of the layer and the supporting semiconductor beneath [29,30]. Finally, molecular probes based on a calix[4]arene benzocrown ether are grafted on the surface of the lipids to ensure the selectivity [34]. We demonstrate, that by playing judiciously with the affinity constants, it allows us to detect cesium in seawater with a high selectivity and a detection limit 5 orders of magnitude lower than for ICP-MS.

2. Materials and methods

2.1 Materials

2-(2-chloroethoxy)ethanol), catechol and *p*-toluenesulfonyl chloride (TsCl) were purchased from TCI. Calix[4]arene and allyl bromide were purchased from Alfa Aesar. P3HT (90% regioregular), Karstedt's catalyst, Li^+, Na^+, K^+, Rb^+, Cs^+, and Mg^{2+} as chlorine salts, dimethylformamide (DMF), anhydrous acetonitrile (CH_3CN), methanol (MeOH), dichloromethane (DCM), tetrahydrofuran (THF), anhydrous toluene, anhydrous 1,4-dioxane, K_2CO_3, NaOH and Cs_2CO_3 were purchased from Sigma Aldrich. All compounds and solvents were used as received. Column chromatography was performed using silica 60 M (0.04-0.063 mm) purchased from Macherey-Nagel. 1,2-bis(10,12-tricosadiynoyl)-*sn*-glycero-3-phosphocholine (DCPC) and Phospholipase C from Bacillus cereus were purchase from Sigma Aldrich.

2.2 Fabrication of transistor

EG-OFETs were fabricated according to the following protocol: first, source and drain gold electrodes were patterned on a 200 nm thick SiO_2/p-Si substrates through a shadow mask by thermal evaporation. The gate area dimensions were 100 µm and 2000 µm respectively for the length (L) and the width (W). Second, a 0.75 wt% solution of P3HT in chlorobenzene was prepared and heated at 60°C for 30 min. and filtered through a 200 nm pore-sized membrane prior to be spin-coated (2000 rpm, 60 sec.) on the patterned substrates. The P3HT film was then annealed at 150°C under vacuum to eliminate the residual solvent. Upon this process edge-on oriented thin

films of P3HT were obtained (~20 nm in thickness) with alkyl chains pointing out of the surface. Finally, a PCTFE container (400 µl) was carefully sealed on the top of the P3HT film. The gate bias voltage was applied by the immersion of an Au gate electrode into the electrolyte solution.

2.3 Lipid monolayer formation

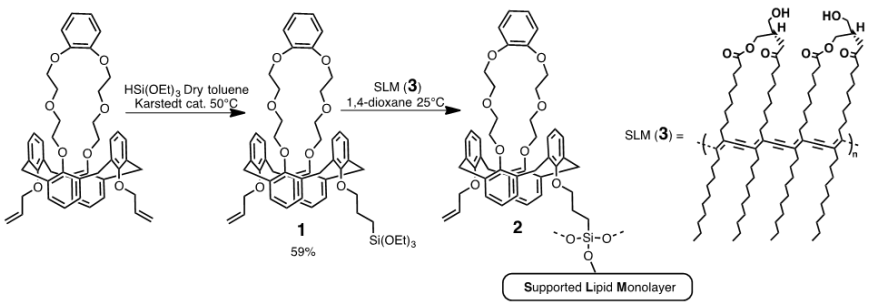

*Scheme 1: DCOH-R lipid layer (**3**) was obtained from DC8,9PC lipids after enzymatic cleavage of their head-groups leaving hydroxyl functions at the head-groups and reticulation of the layer. Grafting of calix[4]arene derivative (**1**) to the lipid layer was obtained by silanization of the -OH groups of DCOH lipids by the triethoxysilane end-group of the probe legs.*

Lipid monolayer was prepared from DCOH lipids. DCOH lipids were synthetized from commercially available DCPC lipids by enzymatic cleavage of the phosphatidylcholine head-group with Phospholipase C according to the following protocol [22]. To a solution of 5 mg DCPC in 50 mL of deionized water, buffered at pH 7.2, was added a catalytic amount of phospholipase C. The reaction mixture was consecutively sonicated over 15 min then slowly stirred at 55°C for 72h. Then, the aqueous phase was extracted three times with chloroform and the organic phase was dried over Mg_2SO_4, filtered and evaporated under reduced pressure. The crude residue was further purified by column chromatography over SiO_2 using petroleum ether 8:2 ethyl acetate as eluent. The solvents were removed under reduced pressure affording DCOH as a white solid in 85 % yield.

Lipid monolayer formation on P3HT was extrapolated from previous work on silicon [32]. A freshly prepared 1 wt% lipid emulsion of DCOH lipid in DI-water was first sonicated during 30 minutes in order to obtain unilamellar vesicles and then extruded through a 100 nm pore-size membrane. The homogeneous DCOH vesicles solution was deposited onto the P3HT film at room temperature. Subsequently, the temperature was lowered to 10°C for 5 min affording the

formation of a stable DCOH lipid monolayer at the P3HT interface through a three-step process involving the condensation, the fusion then the spreading of the vesicles. The result is the formation of a dense monolayer with additional bilayers stacked atop. The latest are desorbed from the monolayer by gradually increasing the temperature from 10°C to 30°C at a rate of 1°C per minute. Additional mechanical stability of the monolayer was further achieved by free-radical polymerization of the unsaturated alkyl lipid chains initiated at 30°C by adding 0.1 w% of azobis(2-amidinopropane dihydrochloride (AAPD) as radical initiator. Reticulation was thermally activated by increasing the temperature up to 42°C at a rate of 5°C per ten minutes and kept at 42°C for 45 minutes. Lastly, the layer was cooled down to room temperature and rinsed with deionized water resulting in a highly stable ultrathin DCOH-R monolayer on P3HT.

2.4 Grafting of cesium probe to lipid layer

The full synthesis of the cesium's probes was described elsewhere, following reported literature procedures for analogous compounds [35–40]. The probes have demonstrated high affinity constants toward Cs^+ (6024 M^{-1}) while for the most competitive ions such as Rb^+ and K^+ the latter was about two-fold magnitude lower respectively (2288 M^{-1}, 2825 M^{-1}) [34]. Note that no affinity was found for Na^+ ions. The probes were ultimately modified using the Karstedt's catalyst in order to introduce a triethoxysilane ($Si(OEt)_3$) group used for their grafting on the top of the DCOH-R monolayer through a silanization-like reaction. The probe **1** was successfully integrated on the single lipid monolayer as follows (Scheme 1): 80 µL of a probe solution at 0.25 M in anhydrous 1,4-dioxane was poured in the PCTFE container and kept during 30 minutes at room temperature. After completion of the reaction the newly functionalized monolayer **2** was successively rinsed several times with 1,4-dioxane then DI water and is ready at this stage to be used in sensing measurements. Note that with a probe **1** molecular area of 120$Å^2$, only a portion of the surface hydroxyl groups are used to bind to the probe. This is further discussed in section §3.1.1.

2.5 Sensing measurements

Transistors characteristics were collected using a semiconductor parameter analyzer (Agilent B1500A) under ambient conditions. The gate voltage (V_{GS}) was applied between a metal (gold) electrode dipped in the analyte solution and the P3HT semiconducting layer. The sensor output signal was determined based on the shift of the threshold voltage (V_{th}) and estimated from the transfer curves (I_{DS} vs V_{GS}) in the saturation regime; V_{GS} was swept from 0 to -300 mV keeping V_{DS}=-300 mV constant (Fig S1). The measuring solution consisted in either buffered or pure NaCl (10 mM) or PBS (150 mM). Solutions containing the ions of interest at concentrations ranging from 0.01 fM to 10 µM were prepared either in DI water or in sea water (0.9 M). All sensing measurements were performed as follows: PCTFE container was filled with 100 µl of NaCl or PBS solution. Then 100 µl of a sample solution at a given concentration was added to the container and mixed to the analyte solution. After 5 min, the container was rinsed with the analyte solution. Transfer curves were then performed using analyte solution as the gate.

2.6 NMR analysis

NMR spectra were recorded on a JEOL ECS400 NMR spectrometer at room temperature. NMR chemical shifts are given in ppm (δ) relative to Me_4Si with solvent resonance used as internal standard ($CDCl_3$ 7.26 ppm for ^1H and 77.7 for ^{13}C). ^1H RMN titrations were conducted in solution in a mixture of $CDCl_3$:MeOD:D_2O deuterated solvents by the gradual addition of an increased number of equivalent for each tested cations (Cs^+, K^+, Rb^+, Na^+) to the probe **1**. Competitive studies were performed under the same conditions by adding a putative competitive cation **M'**$^+$ to a preformed **1**⊂**M**$^+$ complex.

3. Results and discussion

3.1 EG-OFET detection of Cs^+ in solution

3.1.1 Importance of a buffered electrolyte on the sensor response

Selective detection of specific ions by EG-OFETs is generally hampered by the competitive ions present in solutions. We have recently reported that the selected probe **1** exhibits greater affinity for Cs^+ comparatively to K^+ and Rb^+ which turned out to be the two most competitive ions [34]. In a first experiment, we attempted to minimize the effect of ions competition by performing experiments in a 10^{-2} M NaCl electrolyte, Na^+ and Cl^- being the two major ions present in seawater. Two electrolytes were prepared: pure NaCl or buffered NaCl + Na_2HPO_4 solution at pH=7.2. Cs^+ surface chelation was monitored by measuring the I_{DS} versus V_{GS} transfer curves for different Cs^+ concentrations [10 aM – 10 µm] in solutions. Upon the formation of **1**⊂Cs^+ complexes, a surface potential change at the dielectric/solution interface is expected, leading to a modulation of the current flow in the semiconducting channel (I_{DS}) and to a shift of the threshold voltage of the transistor device (V_{th}). All electrical measurements herein were performed in the saturation regime for which I_{DS} is given by the relation $I_{DS} = \frac{1}{2}\frac{W}{L}\mu . C_g . (V_{GS} - V_{th})^2$ with W and L the width and length of the gate area respectively, µ, the carrier mobility in the P3HT layer, and C_g, the gate dielectric capacitance which includes the capacitance of the lipid/probe sensing monolayer (C_{SML}) in series with the double layer capacitance (C_{DL}) in solution (Fig. 1D). As an example, two I_{DS}-V_{GS} transfer curves obtained prior to (blue squares) and after (red triangles) exposure of the sensor to a 1 nM Cs^+ solution are displayed in Fig. 2A). The I_{DS}-V_{GS} transfer curve measured in absence of Cs^+ ([Cs^+] = 0 M) is used to measure the reference of the threshold potential V_{th0}. The trapping of the positively charged Cs^+ ions, induces a decrease of I_{DS} leading to a negative shift of V_{th} (inferred from the extrapolation of the linear fitting of the upper part of the curves). Sensitivity measurements performed in buffered (blue circles) and non-buffered (red squares) NaCl solutions, with concentrations of Cs^+ varying from 10^{-19} to 10^{-5} M, exhibit very different behaviors (Fig. 2B). In buffered solutions the curve shows a linear variation of the threshold potential V_{th} with the logarithm of the concentration over the whole range, with a saturation appearing above 10^{-7} M. In contrast, in non-buffered solutions, only minor variations are observed over the same concentration range evidencing a lack of sensitivity under these conditions, thus highlighting the importance to work in buffered solution. Note that an experiment was also performed in DI-water

indicating no sizeable sensitivity to Cs^+ in these conditions (Fig. S2). This response to pH may originate from the nature and structure of the sensing layer with the presence of pH sensitive functional groups. A protonation of the oxygens from the C-O-C groups in the ether-crown is expected in acidic medium. However, in this case, several works from the literature reporting on the effect of proton and hydronium ions complexation by crown ethers (considered as weak bases), demonstrated lower affinity constants compared to other cations and effective exchanged by the cation of interest when the latter is present in solution [41,42]. Thus, pH should have very minor effect on the capability of the crown ether of the chelator to interact with cesium. The main effect however, is expected from the presence of unreacted free -OH groups remaining atop of the lipid monolayer after the probe anchoring. It was indeed shown that with a molecular area of the cesium probe **1** of 120 $Å^2$, i.e. a maximum surface density of ~5-8 $\times 10^{13}$ probes/cm^2, and assuming a hexagonal close packing of the DCOH lipids, a DCOH-R:**1** ratio of 5:1 is estimated [34]. Also, during the grafting process, the siloxane polymerization step leaves behind some unreacted groups or functions that are also pH sensitive. In these two cases a protonation of the -OH groups, that is expected in acidic conditions such as in water or non-buffered NaCl, may induce a charge screening that may drastically reduce the sensor sensitivity. This hypothesis is supported by previous work where transistors containing DCOH lipid monolayer as gate dielectric demonstrated a linear response of the threshold voltage with the pH which could be cancelled by replacing the -OH groups by a non-reactive CH_3 function [30].

To avoid this pH interference and to ensure that the sensor response is related and sensitive to the target ions, experiments are hence required to be performed in buffered solutions at constant pH. In the next section, all experiments were performed at pH=7.2 using PBS as analyte solution (137 mM NaCl, 2.7 mM KCl, 10 mM Na_2HPO_4, 1.76 mM KH_2PO_4).

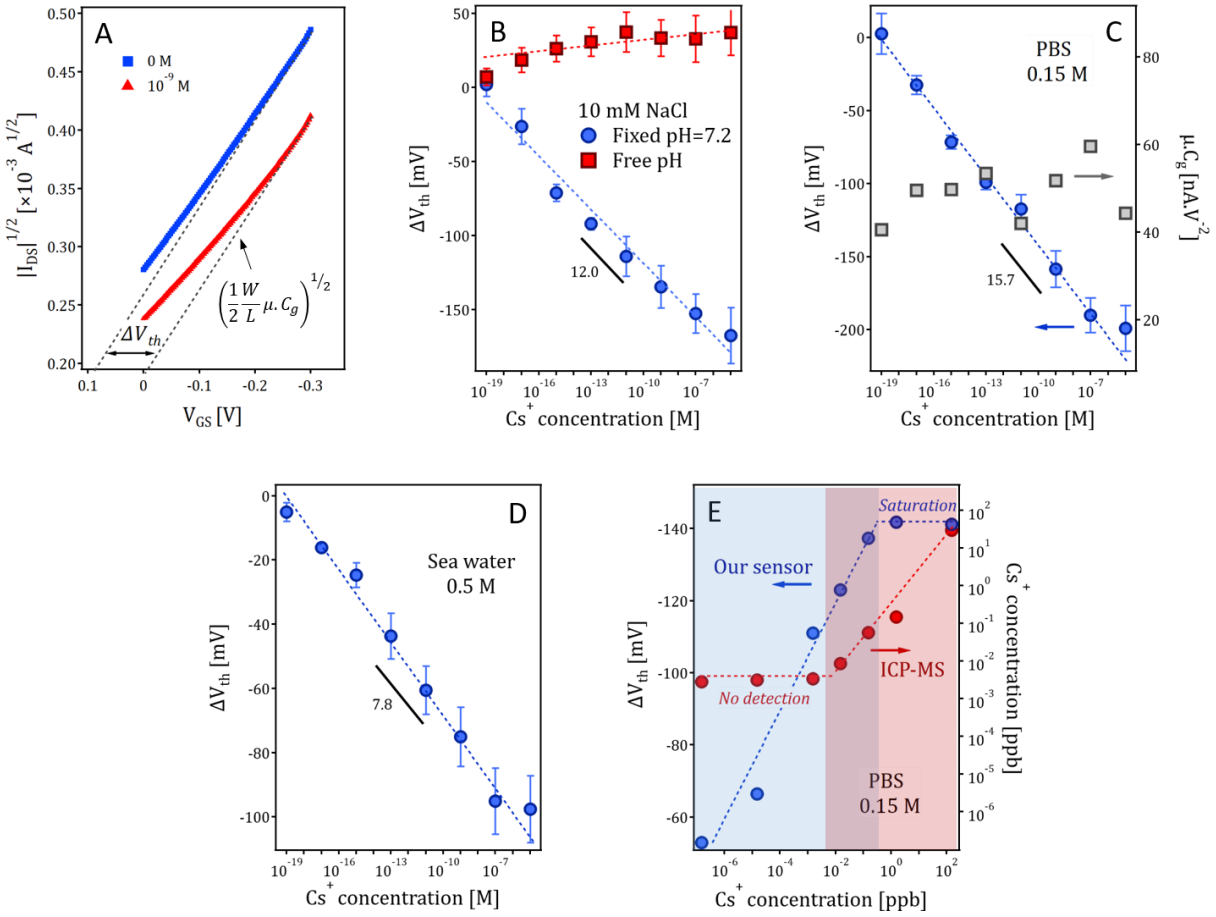

Figure 2: A) Transfer curves obtained in buffered 10 mM NaCl, before (blue) and after (red) exposure of the sensor to 1 nM Cs^+ ions. The threshold voltage V_{th} is obtained by a linear fitting of the top part of the curves. B-D) Sensor sensitivity in various media: Shift of the threshold voltage ΔV_{th} as a function of Cs^+ concentration (in log scale) in non-buffered (red) and pH=7.2 buffered (blue) NaCl solutions (B), in 0.15 M PBS solution (C, blue circles) and in sea water (D). In (B) the grey squares (right Y axis) represent the evolution of the quantity μ×Cg (carrier mobility × dielectric capacitance) inferred from the slope of the transfer curves. Note the variable sensor sensitivity (slope) in the different media: 12 mV/decade in pH=7.2 buffer NaCl, 15.7 mV/decade in 0.15 M PBS and 7.8 mV/decade in sea water. E) Comparison of the performances of EG-OFET sensor (in blue) with ICP-MS based detection (red).

3.1.2 Detection of Cs^+ in PBS and seawater

Seawater is a more complex medium and contains a multitude of ions including K^+ and Rb^+, the two most competitive ions to Cs^+. The greater affinity of probe **1** to Cs^+ compared to its alkali analogs constitute a key parameter for the fabrication of sensors exhibiting high selectivity to Cs^+ even in the seawater. We first started to investigate the impact of high concentrations of K^+ in Cs^+

detection using 1x PBS solution (C_{K+} = 4.5 mM, pH=7.2). Sensing experiments were carried out similarly to the ones in NaCl solutions with Cs^+ concentrations within the 10^{-19} to 10^{-5} M range. Surprisingly, the sensitivity curve shown in Fig. 2C), obtained from the average of 6 different transistors, displays the same linear dependency as was previously obtained in NaCl solutions demonstrating the effective detection of Cs^+ even in presence of high concentrations of competitive cations. The measured sensitivity is 15.7 mV/decade. Note also that the product *carrier mobility × dielectric capacitance* ($\mu \times Cg$, Fig. 2C, grey squares) remains constant over the whole range of concentrations suggesting that neither the dielectric capacitance nor the carrier mobility are effected by the presence of ions in the solution nor by the formation of $\mathbf{1}\subset M^+$ complexes [24].

A similar experiment was performed in seawater using normalized ASTM D665 standard seawater at a concentration of 0.9 M (Seawater composition is given in Table S1). Experiments were conducted in buffered solutions using a 1:1 mixture of 0.15 M PBS and 0.9 M seawater with $[Cs^+]$ in the range of 10^{-19} to 10^{-5} M (Transfer curves are shown in Fig. S3). A linear dependency similar to that observed in NaCl or PBS solutions is observed (Fig. 2D). The sensitivity, 7.8 mV/decade, is lower than in NaCl or PBS. This can be ascertained to charge screening of the charges because of the higher ionic strength of the solution. Interestingly the limit of detection remains unchanged at 10 aM.

3.1.3 Comparison between EG-OFET and ICP-MS.

For the sake of comparison, measurements were carried out in parallel with EG-OFET and ICP-MS (Induction Coupled Plasma-Mass Spectrometry), the most sensitive and commonly used technic for measuring metallic ions quantities in complexed solutions. Fig. 2E compares the performances of both technics using the same set of Cs^+ solutions diluted in 0.15 M PBS. The variations of the threshold voltage ΔV_{th} measured with EG-OFET (blue circles) and the Cs^+ concentration measured by ICP-MS (red circles) are displayed in Figure 2E. The results evidence the complementarity of the two technics with an overlap of detection efficiency within 10^{-2} and 5×10^{-1} ppb range. Below,

ICP-MS is not sensitive and the limit of detection is in agreement with data reported in the literature [9]. Above EG-OFET is saturated. More importantly the limit of detection obtained for the EG-OFET is at least 5 orders of magnitude lower than for ICP-MS making this sensor by far the most sensitive to detect trace amounts of Cs^+ in complex solutions.

3.2 Selectivity towards Cs^+

The above results address the question of the efficient Cs^+ detection even in presence of high concentration of competitive cations. Indeed, the presence of ions such as K^+ in PBS or others cations (K^+, Rb^+, Ca^{2+}, …) in seawater seems to not hinder the Cs^+ detection although in our experiments, an initial probe saturation by K^+ or Rb^+ cations is anticipated that shall prevent efficient detection of Cs^+.

The efficiency and selectivity of our device to Cs^+ can be explained by a greater affinity of the probe for Cs^+ and its ability to substitute other cations with weaker affinity constants (Fig. 3A). This is supported by ^1H NMR investigations of the complexation processes in solution [34]. Fig. 3B shows examples of ^1H NMR spectra of probes **1** in $CDCl_3$:MeOD:D_2O solution prior to (spectrum a) and after addition of one equivalent of K^+, Rb^+, Cs^+ (spectra b-d). In all cases, a shift and a splitting of the multiplets initially standing at ~6.56 and ~6.90 ppm associated to the aromatic protons are observed attesting of the formation of **1⊂M$^+$** complexes. No variation of the NMR spectra is observed in presence of Na^+ (spectrum not shown). Interestingly the shifts and amplitude splitting (differences of chemical shift between the two split components of one multiplet) are different thus providing a specific signature for the complexation of one given cation M^+. The greater affinity of Cs^+ and its ability to substitute the other alkalin cations - in particular K^+ - was demonstrated by carrying out NMR measurements after direct addition of Cs^+ in probe **1** solution (Fig. 3B, spectrum d) or after Cs^+ addition in probe **1** solution previously saturated with K^+ (Fig.3B,

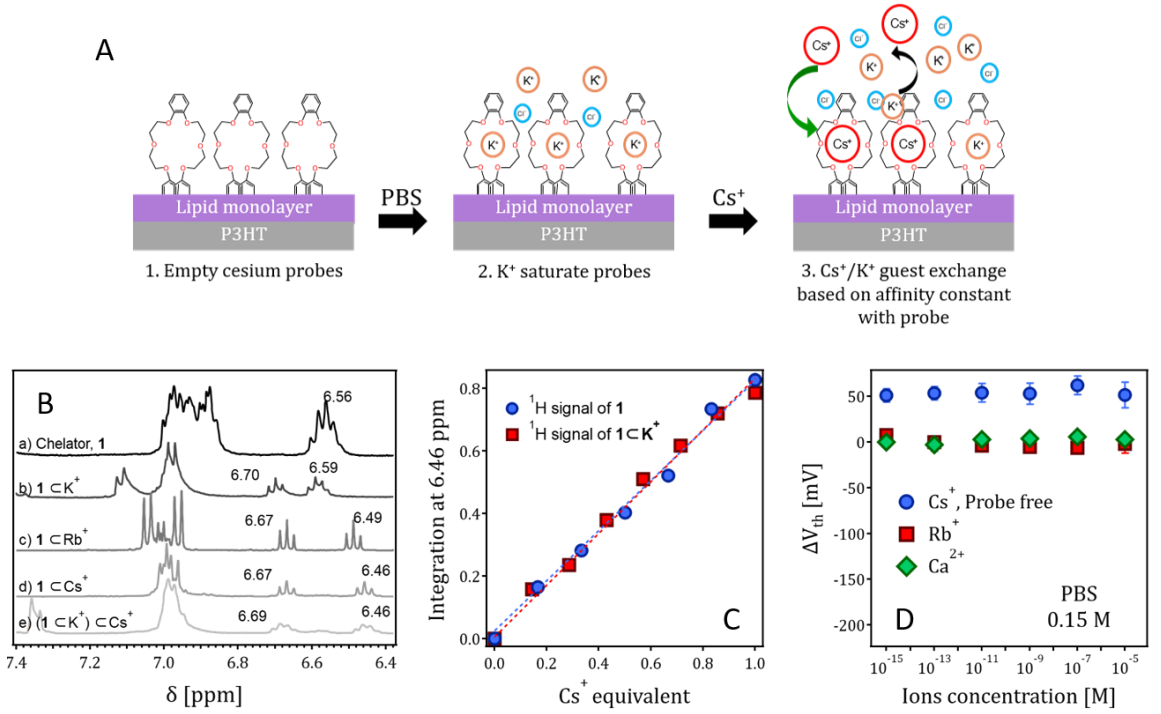

*Figure 3: A) Scheme of guest/host exchange mechanism in presence of K^+ competitive ions in solution driven by the greater affinity constant of probe 1 to Cs^+. B) ^1H RMN spectra of probe **1** in $CDCl_3$:MeOD:D_2O solution prior to (a) and after K^+ (b), Rb^+ (c), Cs^+ (d) molar equivalent addition. C) Job's plot titration: integrated intensity of the calixarene-related multiplet (6.46 ppm) as a function of Cs^+ concentration in the case of the direct addition of Cs^+ in probe **1** solution (blue circles) or after initial saturation of probe **1** by K^+ (red squares). D) Selectivity measurements: Variation of threshold voltage vs the ions concentration for Rb^+ (red squares) and Ca^{2+} (green diamonds) and for Cs^+ using a sensor with no probes grafted to the lipid layer (blue circles).*

spectrum e). In both cases, very similar spectra were obtained indicating an efficient substitution of K^+ ions. The efficient and quantitative Cs^+/ K^+ substitution is further sustained by the Job's plot titration (Fig.3C). In this plot, the integrated intensity of the aromatic protons multiplet at 6.46 ppm is plotted as a function of Cs^+ concentration (from 0 to 1 molar equivalent) in the case of the direct addition of Cs^+ in probe **1** solution (blue circles) or after initial saturation of probes **1** by K^+ (red squares). The two resulting curves are perfectly superimposed confirming a quantitative ion exchange and suggesting that the chelating properties of the probe with Cs^+ are not degraded by prior chelation with another ion.

Although the results discussed above demonstrate a very efficient Cs^+ capture by the probes **1** even in presence of putative competitive ions or when **1⊂M⁺** complexes are already formed, in

homogeneous phase and in organic solvent, the question of the selectivity when the probes are in a different environment (densely packed on a surface and in aqueous medium) as it is the case for OG-FET based detection of Cs^+ in water may be addressed. To investigate this issue specific experiments were carried out.

Firstly, we checked the sensor response in absence of Cs^+ specific probes. For this purpose, the probe **1** atop of the DCOH-R lipid monolayer were replaced by methyl trichlorosilane and the response of the as modified sensor exposed to variable concentrations of Cs^+ was assessed. As expected, no evolution of the threshold potential ΔV_{TH} is observed (Fig. 3D, blue circles) (the shift of the curve to 50 mV is attributed to a small change of the transistor source or drain electrical contact after the reference measurement). Also, this absence of potential variations allows for discarding the contribution of side effects linked to non-specific interactions that could give rise to parasitic electrical output signal.

In a second set of experiments the probes immobilized on the sensor surface were first saturated with K^+ by exposure in PBS solution and then measurements were carried out upon progressive addition of other cations present in the sea water and exhibiting weaker (Ca^{2+}) or similar (Rb^+) affinity for probe **1** (from previous works the following relative affinity strength was determined: **1**⊂Cs^+ > **1**⊂Rb^+ ~ **1**⊂K^+ > **1**⊂Ca^{2+} [34]). As it could be anticipated no variation of the threshold potential V_{th} was measured after the addition of Ca^{2+} (green diamonds) or Rb^+ (red squares) thus confirming the existence of a substitution mechanism driven by affinity similar to that evidenced in homogeneous phase.

3.3 Origin of the limit of detection

In an EG-OFET sensor the complexation of target ion/molecule with the probe receptor induces a response which is translated into the transistor figure of merits. Experimentally the measured response is generally a modification of the threshold potential V_{th} of the device that may be correlated to modifications of the charge distribution at the sensing layer/solution interface induced by complexation events. However other effects as charge screening, modification of the

dielectric properties of the organic gate and/or the electrical properties of the organic semiconductor (charge trapping, modification of carrier mobility) may give rise to a variation of the output signal and hence affect the performances of the sensor in terms of limit of detection (LOD). The purpose here is to discuss the origin of the remarkable LOD in the sub-femtomolar range obtained with this sensor design.

3.3.1 Electrical properties at the interface

A scheme of the sensing layer/solution interface is displayed in Fig. 1D. The active monolayer can be divided in two parts: the dense DCOH lipid monolayer (thickness ~2.2 nm) acting as the dielectric gate and the topmost probe layer whose density is limited by the bulky structure of the calix[4]arene probes. Electrically the interface can be modeled by three serial capacitances: C_{LM} the capacitance of the dense DCOH-R lipid monolayer (thickness $\delta_{LM} \sim 2.2$ nm) whose electrical and mechanical properties [33] let us assume dielectric properties close to those of lipid monolayers in the crystalline state ($C_{LM} \sim 0.9$ µF/cm² [43]), C_{PL} the capacitance of the probe layer at the topmost surface of the lipid layer and C_{DL} the double layer capacitance in solution. Because of its lesser density compared to the lipid monolayer [43], the probe layer (thickness $\delta_{PL} = 1.26$ nm) can be considered as a complex effective medium composed of the organic probes, entrapped ions and water molecules with a capacitance $C_{PL} >> C_{DCOH-R}$. This is within this layer that most of the variations of charge density are expected upon complexation leading to charge compensation on the solution side. The dielectric properties of such an interface are dominated by the dielectric properties of the lipid monolayer which exhibits the smaller capacitance ($C_{LM} << C_{PL}$, C_{DL}). Assuming a dielectric capacitance $C_{gate} \sim C_{LM} \sim 0.9$ µF/cm² the carrier mobility µ can be inferred experimentally from the slope of the I_{DS} *vs* V_G plots. Charge carrier mobility $\mu \sim 5\times10^{-2}$ cm²/V is calculated. This value is in agreement with those generally reported for P3HT thin films (10^{-4} -10^{-1} cm²/V).

Interestingly our result shows that the product $\mu\times C_{gate}$ (carrier mobility × dielectric capacitance) remains almost constant (Fig.2C) indicating a good stability of the device in terms of the dielectric

properties of the organic gate (the lipid monolayer) and/or the electrical properties of the semiconductor P3HT film (no sizeable modification of the carrier mobility or charge trapping). This allows for discarding major contribution of variations of the intrinsic device electrical properties in the output signal of the sensors

3.3.2 Limit of detection in the sub-femtomolar range

The 10 mV potential shift measured for 10 aM concentration cannot be explained only by an increase of the surface charge density due to the charge carried by the Cs^+. As a matter of fact, our results show that Cs^+ trapping takes place through a substitution mechanism meaning that weak variations of the charge density is anticipated in terms of charges carried by the cations, anyway much weaker than in the case of a *direct* chelation process. Furthermore, in our experimental conditions for a 10 aM concentration, the maximum number of Cs^+ that can be captured is ~600 (gate area of 2×10^{-3} cm^2, 100 µl) which is orders of magnitude smaller than the number of ions required for a 10 mV potential shift taking into account charge screening effect in solution. Indeed using the Grahame equation to describe the surface potential at the sensor/solution interface [21,44] and the site binding model that assumes that the density of captured ions at saturation regime must be equal to the density of immobilized probes [45,46], one can calculate that ~10^{10} ions would be required to induce a 10 mV potential shift.

Therefore, other effects should be considered to explain the unexpected amplitude of the potential shift measured at such low concentration. A possible explanation could come from a modification of the charge distribution within the probe layer resulting from molecular conformation changes induced by the ion complexation. Molecular structural rearrangements leading to surface potential modifications are reported in the literature for Self Assembled Monolayers (SAMs) [47,48]. Such effects are reported upon cis/trans photoisomerization of azobenzene [49] or Pd^{2+} complexation/release on bipyridine [50] SAMs on gold. In both cases the active molecules undergo a structural reorganization leading to a change of the amplitude and/or the orientation of their molecular dipole moment with respect to the surface normal. The spatial charge

redistribution induced by external stimuli (light or Pd^{2+} exposure) at the origin of the modifications of the surface potential observed experimentally is also confirmed by DFT calculations.

Relying on these works we may figure out the existence of similar effects upon the Cs^+ complexation by the crown ether probes immobilized at the sensor surface. The occurrence of conformational changes is supported by NMR results showing a splitting of the multiplets corresponding to the aromatic protons from the calix[4]arene (Fig. 3B) and to the protons of the crown ether moiety (Fig. S4) with chemical shifts that depend on the nature/size of the alkali cation. Molecular reorganization within the probe monolayer was tentatively investigated by ATR-FTIR spectroscopy using polarized IR beam. Unfortunately no polarization effect could be evidenced because of the complexity of the FTIR spectra in the region where specific bands of the crown ether and calix[4]arene are expected. Only a slight intensity decrease of some bands assigned to the calix[4]arene was detected after Rb^+ capture and its subsequent substitution by Cs^+ (Fig. S5). Because of the strong overlapping of the ν_{CO} bands of the crown ether with bands assigned to other components of the sensing layer (ester, siloxane, phenyl) it turned out difficult to make quantitative analysis of the dichroic ratio and therefore get insights in a possible reorientation of the probe **1** molecular dipoles.

In addition to charge redistribution due to individual complexation events, collective effects might also be figured out. In recent works, the FET-based detection of single protein was demonstrated using centimeter square transistor gate. To explain the high sensitivity of the device a model is proposed involving a local modification of the electrical work function at the protein recognition site then propagating laterally through a domino cascade within domains in the sensing layer [51,52]. In our system, the probes are bound to a dense lipid layer through a short carbonyl chain end-capped with a silane function which provides flexibility to the probes orientation on the lipid layer. The probes are supposedly densely packed and their orientation and organization is expected to be governed by the calix[4]arene groups through their interaction through their phenyl rings. In such a configuration collective effects initiated by localized structural molecular

reorganization induced by a single complexation events might also contribute to the surface potential change measured experimentally.

4. Conclusions

In this study we have demonstrated that by controlling affinity driven guest/host ion exchange, one can lift the general problem of selectivity in complexed analytes encountered in all FET-based ion sensors. In our device the pre-saturation of the probes by K^+ ions, prevents the chelation of all other ions except for the most competitive Cs^+ ensuring a great selectivity. With this method, the selectivity is obtained even in very complexed solutions containing competitive ions in high concentration and high ionic strength such as in PBS or seawater. In addition to selectivity, the structure of the sensor using nanometric semiconducting and organic dielectric layers provided extremely low limit of detection in the sub-femtomolar range, at least 5 orders of magnitude lower than that of ICP-MS. These results are very promising, and the integration of such EG-OFET sensor into portable devices could allow fast and low-cost monitoring of Cs^+ in natural waters but also in soils. This unique combination of properties and strategy makes this device a system of choice for the foreseen applications and can be applied for the detection of any kind of ions.

CREDIT AUTHORSHIP CONTRIBUTION STATEMENT

Tin Phan Nguy: Device fabrication, sensing measurements and data analysis. Volkan Kilinc: Probe synthesis and lipid layer engineering, FTIR and sensing measurements. Ryoma Hayakawa: Electrical measurements and analysis. Catherine Henry-De-Villeneuve: FTIR measurements and analysis, writing. Jean-Manuel Raimundo: Chemistry conceptualization, investigation and supervision, data analysis. Yutaka Wakayama: Conceptualization, supervision, data analysis. Anne Charrier: Conceptualization, supervision, data analysis, writing- original draft. All authors reviewed and edited the manuscript.

DECLARATION OF COMPETING INTEREST

The authors declare that they have no known competing financial interests or personal relationships that could have appeared to influence the work reported in this paper.

ACKNOWLEDGEMENTS

This research was performed under the framework of the Strategic International Collaborative Research Program (SICORP) supported by the Japan Science and Technology Agency (JST) and L'Agence Nationale de la Recherche (ANR) under project N°ANR-16-JTIC-0003-01, and was supported by the World Premier International Center (WPI) for Materials Nanoarchitectonics (MANA) of the National Institute for Materials Science (NIMS), Tsukuba.

APPENDIX A.

Supplementary data Supplementary data to this article can be found online at …..

BIBLIOGRAPHY

[1] A. Burger, I. Lichtscheidl, Stable and radioactive cesium: A review about distribution in the environment, uptake and translocation in plants, plant reactions and plants' potential for bioremediation, Sci. Total Environ. 618 (2018) 1459–1485. https://doi.org/10.1016/j.scitotenv.2017.09.298.

[2] S.R. Hart, K, Rb, Cs contents and K/Rb, K/Cs ratios of fresh and altered submarine basalts, Earth Planet. Sci. Lett. 6 (1969) 295–303. https://doi.org/10.1016/0012-821X(69)90171-X.

[3] M. Aoyama, M. Fukasawa, K. Hirose, Y. Hamajima, T. Kawano, P.P. Povinec, J.A. Sanchez-Cabeza, Cross equator transport of 137Cs from North Pacific Ocean to South Pacific Ocean (BEAGLE2003 cruises), Prog. Oceanogr. 89 (2011) 7–16. https://doi.org/10.1016/j.pocean.2010.12.003.

[4] J. Kameník, H. Dulaiova, F. Šebesta, K. Šťastná, Fast concentration of dissolved forms of cesium radioisotopes from large seawater samples, J. Radioanal. Nucl. Chem. 296 (2013) 841–846. https://doi.org/10.1007/s10967-012-2007-4.

[5] H. Kaeriyama, Oceanic dispersion of Fukushima-derived radioactive cesium: a review, Fish. Oceanogr. 26 (2017) 99–113. https://doi.org/10.1111/fog.12177.

[6] M. Aoyama, Long-range transport of radiocaesium derived from global fallout and the Fukushima accident in the Pacific Ocean since 1953 through 2017—Part I: Source term and surface transport, J. Radioanal. Nucl. Chem. 318 (2018) 1519–1542. https://doi.org/10.1007/s10967-018-6244-z.

[7] E.D. van Asselt, H.J. van der Fels-Klerx, H.J.P. Marvin, H. van Bokhorst-van de Veen, M.N. Groot, Overview of Food Safety Hazards in the European Dairy Supply Chain, Compr. Rev. Food Sci. Food Saf. 16 (2017) 59–75. https://doi.org/10.1111/1541-4337.12245.

[8] M. Sangiorgi, M. Angel Hernández Ceballos, G. Iurlaro, G. Cinelli, M. De Cort, 30 years of European Commission Radioactivity Environmental Monitoring data bank (REMdb) - An open door to boost environmental radioactivity research, Earth Syst. Sci. Data. 11 (2019) 589–601. https://doi.org/10.5194/essd-11-589-2019.

[9] A. Alimonti, G. Forte, S. Spezia, A. Gatti, G. Mincione, A. Ronchi, P. Bavazzano, B. Bocca, C. Minoia, Uncertainty of inductively coupled plasma mass spectrometry based measurements: An application to the analysis of urinary barium, cesium, antimony and tungsten, Rapid Commun. Mass Spectrom. 19 (2005) 3131–3138. https://doi.org/10.1002/rcm.2180.

[10] T. Takahashi, Standard limits for radionuclides in foods, J. Food Hyg. Soc. Japan. 54 (2013) 97–101. https://doi.org/10.3358/shokueishi.54.97.

[11] N. Kumar, I. Leray, A. Depauw, Chemically derived optical sensors for the detection of cesium ions, Coord. Chem. Rev. 310 (2016) 1–15. https://doi.org/10.1016/j.ccr.2015.11.008.

[12] I. Leray, B. Valeur, Calixarene-based fluorescent molecular sensors for toxic metals, Eur. J. Inorg. Chem. (2009) 3525–3535. https://doi.org/10.1002/ejic.200900386.

[13] J. Qiu, L. Fu, H. Wang, R. Zou, Y. Zhang, X. Li, A. Wu, Colorimetric detection of Cs+ based on the nonmorphological transition mechanism of gold nanoparticles in the presence of Prussian blue, New J. Chem. 44 (2020) 2241–2246. https://doi.org/10.1039/c9nj05301h.

[14] S.M. Kang, S.C. Jang, Y. Haldorai, A.T.E. Vilian, M. Rethinasabapathy, C. Roh, Y.K. Han, Y.S. Huh, Facile fabrication of paper-based analytical devices for rapid and highly selective colorimetric detection of cesium in environmental samples, RSC Adv. 7 (2017) 48374–48385. https://doi.org/10.1039/c7ra08444g.

[15] M. Akamatsu, H. Komatsu, A. Matsuda, T. Mori, W. Nakanishi, H. Sakai, J.P. Hill, K. Ariga, Visual detection of Cesium ions in domestic water supply or seawater using a nano-optode, Bull. Chem. Soc. Jpn. 90 (2017) 678–

683. https://doi.org/10.1246/bcsj.20170046.

[16] B. Radaram, T. Mako, M. Levine, Sensitive and selective detection of cesium via fluorescence quenching, Dalt. Trans. 42 (2013) 16276–16278. https://doi.org/10.1039/c3dt52215f.

[17] J.B. Joffrion, D. Mills, W. Clower, C.G. Wilson, On-chip microplasmas for the detection of radioactive cesium contamination in seawater, Micromachines. 8 (2017). https://doi.org/10.3390/mi8090259.

[18] M. Saadat, A. Nezamzadeh-Ejhieh, Clinoptilolite nanoparticles containing HDTMA and Arsenazo III as a sensitive carbon paste electrode modifier for indirect voltammetric measurement of Cesium ions, Electrochim. Acta. 217 (2016) 163–170. https://doi.org/10.1016/j.electacta.2016.09.084.

[19] M. Shamsipur, M. Asgari, M.G. Maragheh, D. Matt, Impedimetric sensing of cesium ion based on a thiacalix[4]arene self-assembled gold electrode, Sensors Actuators, B Chem. 209 (2015) 9–14. https://doi.org/10.1016/j.snb.2014.11.047.

[20] N. Alghamdi, Z. Alqahtani, M. Grell, Sub-nanomolar detection of cesium with water-gated transistor, J. Appl. Phys. 126 (2019). https://doi.org/10.1063/1.5108730.

[21] T.D. Nguyen, A. Labed, R. El Zein, S. Lavandier, F. Bedu, I. Ozerov, H. Dallaporta, J.M. Raimundo, A.M. Charrier, A field effect transistor biosensor with a γ-pyrone derivative engineered lipid-sensing layer for ultrasensitive Fe3+ ion detection with low pH interference, Biosens. Bioelectron. 54 (2014) 571–577. https://doi.org/10.1016/j.bios.2013.11.051.

[22] T. Nguyen Duc, R. El Zein, J.M. Raimundo, H. Dallaporta, A.M. Charrier, Label free femtomolar electrical detection of Fe(iii) ions with a pyridinone modified lipid monolayer as the active sensing layer, J. Mater. Chem. B. 1 (2013) 443–446. https://doi.org/10.1039/c2tb00438k.

[23] A. Kenaan, F. Brunel, J.M. Raimundo, A.M. Charrier, Femtomolar detection of Cu2+ ions in solution using super-Nernstian FET-sensor with a lipid monolayer as top-gate dielectric, Sensors Actuators, B Chem. 316 (2020). https://doi.org/10.1016/j.snb.2020.128147.

[24] M. Di Lauro, M. Berto, M. Giordani, S. Benaglia, G. Schweicher, D. Vuillaume, C.A. Bortolotti, Y.H. Geerts, F. Biscarini, Liquid-Gated Organic Electronic Devices Based on High-Performance Solution-Processed Molecular Semiconductor, Adv. Electron. Mater. 3 (2017). https://doi.org/10.1002/aelm.201700159.

[25] S. Cotrone, M. Ambrico, H. Toss, M.D. Angione, M. Magliulo, A. Mallardi, M. Berggren, G. Palazzo, G. Horowitz, T. Ligonzo, L. Torsi, Phospholipid film in electrolyte-gated organic field-effect transistors, Org. Electron. 13 (2012) 638–644. https://doi.org/10.1016/j.orgel.2012.01.002.

[26] F. Buth, A. Donner, M. Sachsenhauser, M. Stutzmann, J.A. Garrido, Biofunctional electrolyte-gated organic field-effect transistors, Adv. Mater. 24 (2012) 4511–4517. https://doi.org/10.1002/adma.201201841.

[27] F. Buth, D. Kumar, M. Stutzmann, J.A. Garrido, Electrolyte-gated organic field-effect transistors for sensing applications, Appl. Phys. Lett. 98 (2011). https://doi.org/10.1063/1.3581882.

[28] O. Knopfmacher, M.L. Hammock, A.L. Appleton, G. Schwartz, J. Mei, T. Lei, J. Pei, Z. Bao, Highly stable organic polymer field-effect transistor sensor for selective detection in the marine environment, Nat. Commun. 5 (2014) 2954. https://doi.org/10.1038/ncomms3954.

[29] T.P. Nguy, R. Hayakawa, V. Kilinc, M. Petit, J.-M. Raimundo, A. Charrier, Y. Wakayama, Stable operation of water-gated organic field-effect transistor depending on channel flatness, electrode metals and surface treatment, Jpn. J. Appl. Phys. 58 (2019) SDDH02. https://doi.org/10.7567/1347-4065/ab09d2.

[30] T.P. Nguy, R. Hayakawa, V. Kilinc, M. Petit, S.L.V.N. Yemineni, M. Higuchi, J.-M. Raimundo, A.M. Charrier, Y. Wakayama, Electrolyte-gated-organic field effect transistors functionalized by lipid monolayers with tunable pH sensitivity for sensor applications, Appl. Phys. Express. 13 (2020) 011005. https://doi.org/10.7567/1882-0786/ab5322.

[31] A. Charrier, T. Mischki, G.P. Lopinski, Direct stabilization of a phospholipid monolayer on H-terminated silicon, Langmuir. 26 (2010) 2538–2543. https://doi.org/10.1021/la9028063.

[32] R. El Zein, H. Dallaporta, A.M. Charrier, Supported lipid monolayer with improved nanomechanical stability: Effect of polymerization, J. Phys. Chem. B. 116 (2012) 7190–7195. https://doi.org/10.1021/jp302306r.

[33] A. Kenaan, R. El Zein, V. Kilinc, S. Lamant, J.-M. Raimundo, A.M. Charrier, Ultrathin Supported Lipid Monolayer with Unprecedented Mechanical and Dielectric Properties, Adv. Funct. Mater. 28 (2018) 1801024. https://doi.org/10.1002/adfm.201801024.

[34] V. Kilinc, C. Henry-de-Villeneuve, T.P. Nguy, Y. Wakayama, A.M. Charrier, J.-M. Raimundo, Novel and Innovative Interface as Potential Active Layer in Chem-FET Sensor Devices for the Specific Sensing of Cs +, ACS Appl. Mater. Interfaces. 11 (2019) 47635–47641. https://doi.org/10.1021/acsami.9b18188.

[35] J.S. Kim, J.H. Pang, I.Y. Yu, W.K. Lee, I.H. Suh, J.K. Kim, M.H. Cho, E.T. Kim, D.Y. Ra, Calix[4]arene dibenzocrown ethers as caesium selective extractants, J. Chem. Soc. Perkin Trans. 2. (1999) 837–846. https://doi.org/10.1039/a808499h.

[36] J.S. Kim, I.Y. Yu, J.H. Pang, J.K. Kim, Y.I. Lee, K.W. Lee, W.Z. Oh, New Calix[4]arene Dibenzocrown Ethers for Selective Sensing of Cesium Ion in an Aqueous Environment, Microchem. J. 58 (1998) 225–235.

https://doi.org/10.1006/mchj.1997.1545.

[37] H.F. Ji, R. Dabestani, G.M. Brown, R.L. Hettich, Synthesis and sensing behavior of cyanoanthracene modified 1,3-alternate calix[4]benzocrown-6: A new class of Cs+ selective optical sensors, J. Chem. Soc. Perkin Trans. 2. (2001) 585–591. https://doi.org/10.1039/b007507h.

[38] K. Wright, F. Melandri, C. Cannizzo, M. Wakselman, J.P. Mazaleyrat, New crown-carrier Cα,α-disubstituted glycines derived from α-methyl-(L)-DOPA, Tetrahedron. 58 (2002) 5811–5820. https://doi.org/10.1016/S0040-4020(02)00566-5.

[39] A.B.C. Deutman, J.M.M. Smits, R. De Gelder, J.A.A.W. Elemans, R.J.M. Nolte, A.E. Rowan, Strong induced-fit binding of viologen and pyridine derivatives in adjustable porphyrin cavities, Chem. - A Eur. J. 20 (2014) 11574–11583. https://doi.org/10.1002/chem.201402919.

[40] M. Surowiec, R. Custelcean, K. Surowiec, R.A. Bartsch, Mono-ionizable calix[4]arene-benzocrown-6 ligands in 1,3-alternate conformations: synthesis, structure and silver(I) extraction, Tetrahedron. 65 (2009) 7777–7783. https://doi.org/10.1016/j.tet.2009.07.006.

[41] I.M. Kolthoff, W.J. Wang, M.K. Chantooni, W.J. Wang, Protonation and Hydronium Complexation Stability Constants of Several Crown Ethers in Acetonitrile, Anal. Chem. 55 (1983) 1202–1204. https://doi.org/10.1021/ac00259a005.

[42] H.J. Buschmann, Complexation of protons by macrocyclic polyethers in acetonitrile, Polyhedron. 6 (1987) 1469–1472. https://doi.org/10.1016/S0277-5387(00)80911-0.

[43] V.R. Ardham, V. Zoni, S. Adamowicz, P. Campomanes, S. Vanni, Accurate Estimation of Membrane Capacitance from Atomistic Molecular Dynamics Simulations of Zwitterionic Lipid Bilayers, J. Phys. Chem. B. 124 (2020) 8278–8286. https://doi.org/10.1021/acs.jpcb.0c03145.

[44] T. Uno, H. Tabata, T. Kawal, Peptide-nucleic acid-modified ion-sensitive field-effect transistor-based biosensor for direct detection of DNA hybridization, Anal. Chem. 79 (2007) 52–59. https://doi.org/10.1021/ac060273y.

[45] D.E. Yates, S. Levine, T.W. Healy, Site-binding model of the electrical double layer at the oxide/water interface, J. Chem. Soc. Faraday Trans. 1 Phys. Chem. Condens. Phases. 70 (1974) 1807–1818. https://doi.org/10.1039/F19747001807.

[46] R.E.G. van Hal, J.C.T. Eijkel, P. Bergveld, A novel description of ISFET sensitivity with the buffer capacity and double-layer capacitance as key parameters, Sensors Actuators B. Chem. 24 (1995) 201–205. https://doi.org/10.1016/0925-4005(95)85043-0.

[47] J. Lü, E. Delamarche, L. Eng, R. Bennewitz, E. Meyer, H.J. Güntherodt, Kelvin probe force microscopy on surfaces: investigation of the surface potential of self-assembled monolayers on gold, Langmuir. 15 (1999) 8184–8188. https://doi.org/10.1021/la9904861.

[48] H. Sugimura, N. Saito, N. Maeda, I. Ikeda, Y. Ishida, K. Hayashi, L. Hong, O. Takai, Surface potential microscopy for chemistry of organic self-assembled monolayers in small domains, Nanotechnology. 15 (2004). https://doi.org/10.1088/0957-4484/15/2/015.

[49] A. V. Zakharov, D. Taguchi, T. Manaka, M. Iwamoto, Monolayer alignment on azobenzene surfaces during UV light irradiation: Analysis of optical polarized absorption measurement results and theoretical treatment, J. Chem. Phys. (2006). https://doi.org/10.1063/1.2141956.

[50] T. Nakamura, E. Koyama, Y. Shimoi, S. Abe, T. Ishida, K. Tsukagoshi, W. Mizutani, H. Tokuhisa, M. Kanesato, I. Nakai, H. Kondoh, T. Ohta, Surface potential switching by metal ion complexation/decomplexation using bipyridinethiolate monolayers on gold, J. Phys. Chem. B. 110 (2006) 9195–9203. https://doi.org/10.1021/jp056821d.

[51] E. Macchia, K. Manoli, C. Di Franco, R.A. Picca, R. Österbacka, G. Palazzo, F. Torricelli, G. Scamarcio, L. Torsi, Organic Field-Effect Transistor Platform for Label-Free, Single-Molecule Detection of Genomic Biomarkers, ACS Sensors. 5 (2020) 1822–1830. https://doi.org/10.1021/acssensors.0c00694.

[52] P. Seshadri, K. Manoli, N. Schneiderhan-Marra, U. Anthes, P. Wierzchowiec, K. Bonrad, C. Di Franco, L. Torsi, Low-picomolar, label-free procalcitonin analytical detection with an electrolyte-gated organic field-effect transistor based electronic immunosensor, Biosens. Bioelectron. 104 (2018) 113–119. https://doi.org/10.1016/j.bios.2017.12.041.